NANO LETTERS

pubs.acs.org/NanoLett Letter

Tunable Nanochannels Connected in Series for Dynamic Control of Multiple Concentration-Polarization Layers and Preconcentrated Molecule Plugs

Barak Sabbagh, Elad Stolovicki, Sinwook Park, David A. Weitz, and Gilad Yossifon*

Cite This: *Nano Lett.* 2020, 20, 8524–8533 Read Online

ACCESS | Metrics & More | Article Recommendations | Supporting Information

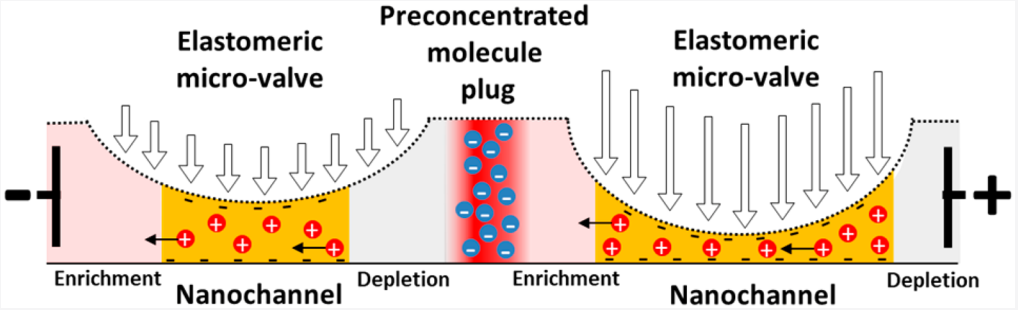

ABSTRACT: Integration of ionic permselective medium (e.g., nanochannels, membranes) within microfluidic channels has been shown to enable on-chip desalination, sample purification, bioparticle sorting, and biomolecule concentration for enhanced detection sensitivity. However, the ion-permselective mediums are generally of fixed properties and cannot be dynamically tuned. Here we study a microfluidic device consisting of an array of individually addressable elastic membranes connected in series on top of a single microfluidic channel that can be deformed to locally reduce the channel cross-section into a nanochannel. Dynamic tunability of the ion-permselective medium, as well as controllability of its location and ionic permselectivity, introduces a new functionality to microfluidics-based lab-on-a-chip devices, for example, dynamic localization of preconcentrated biomolecule plugs at different sensing regions for multiplex detection. Moreover, the ability to simultaneously form a series of preconcentrated plugs at desired locations increases parallelization of the system and the trapping efficiency of target analytes.

KEYWORDS: *Electrokinetics, nanofluidics, concentration-polarization, preconcentration, pneumatic microvalve*

INTRODUCTION

The ion permselectivity of a medium (e.g., membrane, nanochannels) to the transport of ions of a given charge is an intriguing physical phenomenon. Its potential applications include electrochemical separation (e.g., direct seawater desalination and purification),[1−4] energy harvesting (e.g., reverse electrodialysis and streaming current/potential),[5−9] ionic circuit components (e.g., diodes, transistors, and inductors),[10−13] and biomolecule preconcentration for enhanced biosensing in lab-on-a-chip format.[14−24] Interestingly, a medium with a pore size of several orders of magnitude larger than the ions becomes ion permselective due to ion interaction with the pore surface charges. The ions screen the surface charges and form an electric-double layer (EDL) wherein there is an excess of counterions distributed according to Boltzmann statistics, with a characteristic Debye length (λ_D).[25] Moreover, reduction of the pore size to similar dimensions as the Debye length causes an overlap of the EDLs, which leads to the exclusion effect of co-ions and the preferential permeability of counterions (i.e., ions of a charge opposite that of the surface) and gives rise to a Donnan potential within the pore.[26]

The selectivity of the pore to transport of counterions, thereby leading to a symmetry-breaking phenomenon, causes the formation of ion-depleted and -enriched diffuse layers at the opposite sides of the pore inlets upon the application of an electric field. This electrokinetic phenomenon is termed concentration-polarization (CP).[27−30] Intriguingly, the ion concentration gradient caused by the CP creates electric field gradients that can trap and concentrate charged molecules into a preconcentrated plug at the edge of the ion-depleted layer. This ability to harness CP to concentrate molecules of interest on-chip has the potential to improve the detection of biomolecules within a small volume and of low concentration.[16,21]

Received: July 20, 2020
Revised: October 27, 2020
Published: November 23, 2020

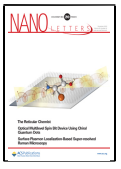

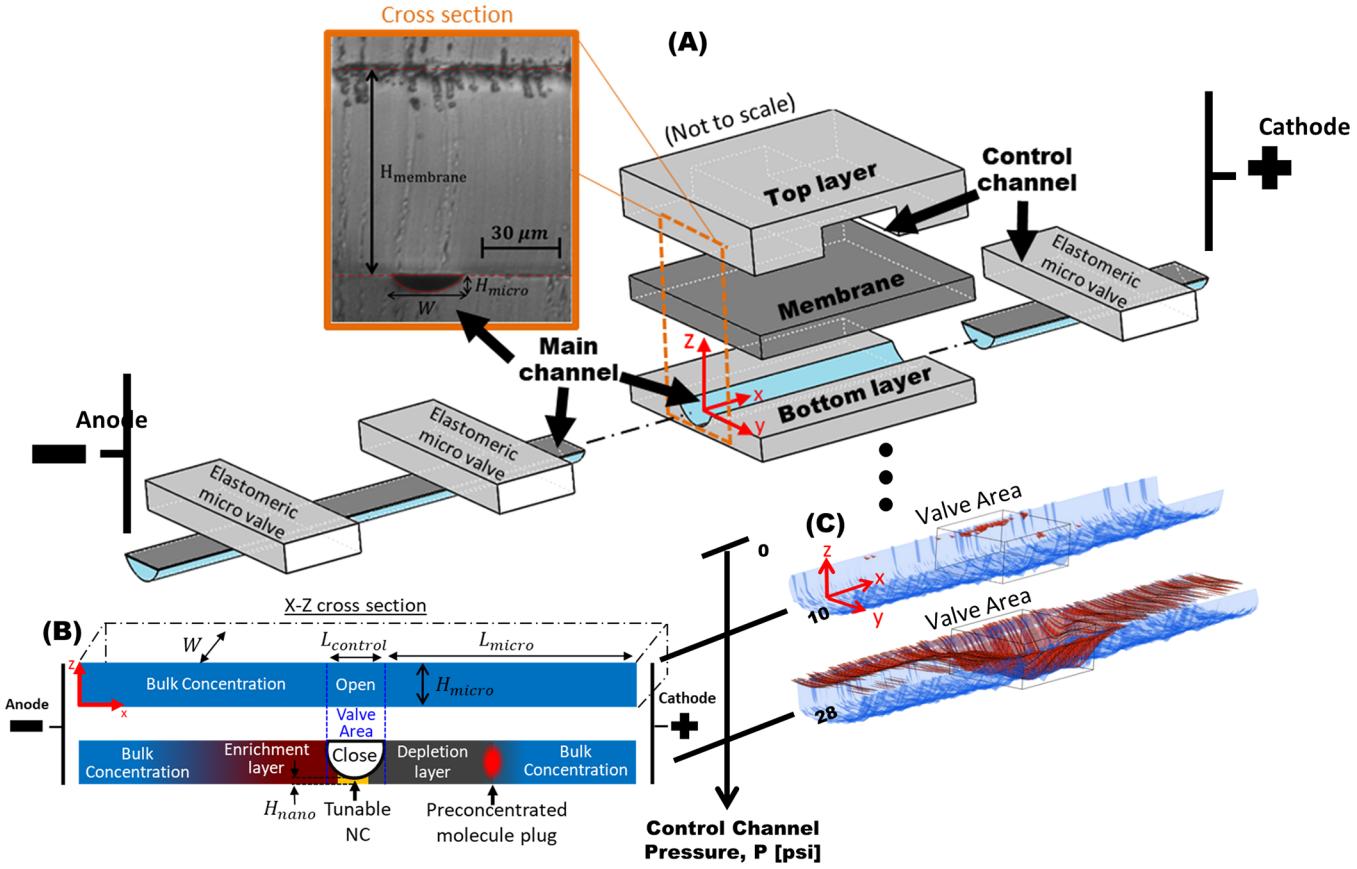

Figure 1. (A) Schematic description of the chip layout consisting of three bonded PDMS layers. The bottom layer contains the main microfluidic channel, into which the solution is introduced. The intermediate layer acts as a deformable membrane (i.e., microvalve) that can block the main channel under application of pressure in the control channel. The top layer contains the control channel with a pressurized fluid. Orange rectangle inset—cross-sectional view of the chip layers. (B) Schematics of the concentration-polarization phenomenon for the open and closed valve, where the background colors indicate the cation (C+) and anion (C−) concentrations for cation exchange NC (black, $C_{\pm} \approx 0$; blue, $C_{\pm} = C_0$, dark red, $C_{\pm} > C_0$, bright red, analyte concentration $C_3 \gg C_0$). (C) 3D reconstruction of the membrane deformation, obtained using confocal microscopy. The red surface is the bottom membrane surface and the blue plane is the main channel wall. The channel was scanned at an overpressure (relative to the ambient pressure) of 0 psi, to determine the reference geometry onto which the membrane deformation under varying channel pressures was superimposed. The open and closed valve cases are depicted for P = 10 psi and P = 28 psi, respectively (for more details, see Supplementary Figure S1 and Supplementary Video S1).

Enhancing the sensitivity of detection in CP-based devices requires a precise overlap between the preconcentrated biomolecule plug and the specific molecular probes (e.g., antibodies). However, extensive precalibration is required to predict the plug location since it depends on various system parameters (e.g., flow rate, electric field, channel geometry, pH). One approach to control the location of the biomolecule plug in a direct and dynamic manner uses embedded electrodes for local stirring of the fluid, driven by alternating-current electro-osmosis (ACEO).[31] Unfortunately, this method is limited to relatively low conductivity solution (<0.1 S/m). Another recent approach uses electrothermal (ET) local stirring to control the length of the ion-depleted layer and, thus, the location of the preconcentrated analyte plug.[32,33]

Permselective pores are often fabricated by etching nanochannels (NCs) on a hard substrate, for example, silicon or glass.[34−36] However, these fixed-geometry NCs (e.g., height) cannot be tuned on demand. To overcome this challenge, a dynamically tunable NC can be made from soft elastomer, where the cross-section dimensions of the channel are changeable from micro- to nanometer scale, thereby switching the channel from an open microchannel to an ionic permselective nanochannel.[37−40] Yet, with all its advantages, a single tunable NC does not enable the control of the preconcentrated plug position. Herein, we introduce a simple method for tuning the system performance (i.e., ion perm selectivity, solvent permeability) of a single tunable NC by varying the channel cross-sectional dimension in a continuous manner, thereby, enabling its optimization and dynamic operation. Furthermore, we assessed use of an array of individually controlled tunable NCs connected in series, to control the location of the preconcentrated plug. The array of tunable NCs can also form multiple biomolecule traps, which is of great potential for enhanced parallelization of biosensing as well as multiplexing. In addition, we demonstrated that such an array of serially connected traps has higher trapping efficiency, since analyte molecules that escape the first trap can be trapped in a downstream trap.

RESULTS

Serial Array of Tunable Nanochannels. The array of tunable NCs is comprised of several microvalves connected in series, each individually controlled by a designated control channel and deformable membrane. An electric field is applied using electrodes that are immersed within the inlet reservoirs,

https://dx.doi.org/10.1021/acs.nanolett.0c02973
Nano Lett. 2020, 20, 8524−8533

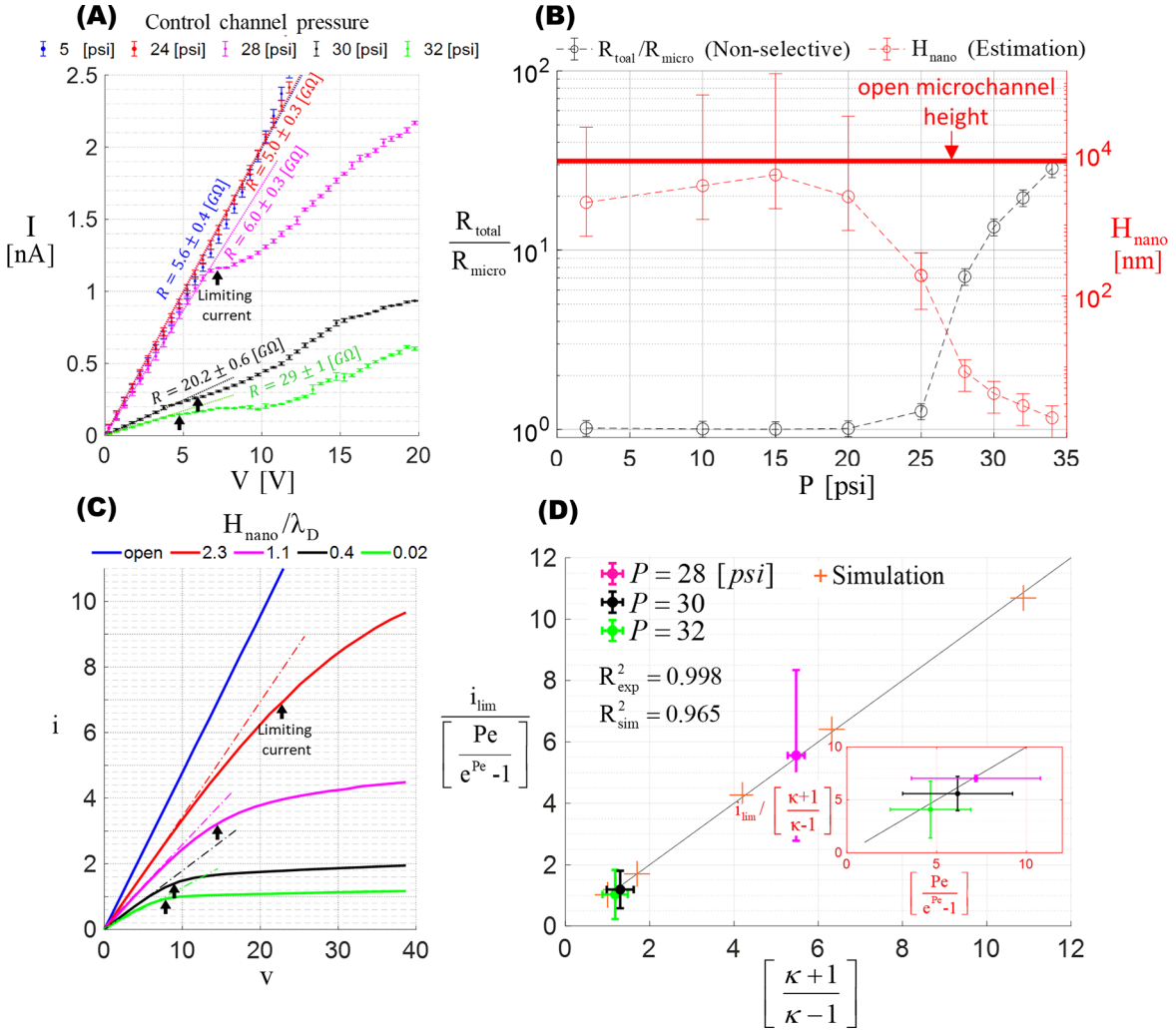

Figure 2. Characterization of a single tunable NC response under varying control channel pressures. (A) Experimentally measured current−voltage curves for varying control channel pressures. A ∼0.65 mM KCl solution (σ = 97 μS/cm) and a voltage-sweeping rate of 10 mV/s were used. The ohmic resistance was estimated based on the curve slope under the limiting current (indicted by black arrows). (B) Estimation of the NC height for different control channel pressures. The normalized ohmic resistance versus control channel pressure for high concentration (120 mM, σ = 1.8 S/m) KCl solution, resulting in a nonselective NC, is depicted on the left y-axis (black line). The estimated NC height is depicted on the right y-axis. The red line represents the MC height for an open valve. (C) Calculated normalized current density−voltage response for varying NC heights using a 1D numerical simulation model. (D) Ratio of the normalized limiting current density (i_{lim}) to the EOF-based advection dependency ($Pe/(e^{Pe} - 1)$) versus the nonideal ionic permselectivity dependency ($((\kappa + 1)/(\kappa - 1))$, where the solid line stands for a linear behavior as described in the scaling relation. Both experimental and numerical values collapse on this linear trend with coefficient of determination of R_{exp}^2 = 0.998 and R_{sim}^2 = 0.965, respectively. The EOF-based dependency on the normalized limiting current density over the nonideal ionic selectivity dependency is shown in the inset. The ohmic resistance, electrical current, and voltage are normalized by the theoretical resistance of the open microchannel (R_{micro}), 1D limiting current density of an ideal permselective medium, and thermal voltage, respectively (for more details, see description in Supporting Information, numerical simulation section).

resulting in CP along the microchannel (MC) when the tunable NC is activated, as shown in Figure 1.

Characterization of the Quasi-Steady-State Behavior of a Single Tunable Nanochannel. Characterization of the device was initiated by studying a single tunable NC. Specifically, the transition of a channel from nonselective to permselective for ion transport, by simply changing the channel dimensions from micrometers to few nanometers, was assessed. Precise control of the channel dimensions can be achieved by applying pressure on the membrane of the elastomeric microvalve. As a result, the membrane deforms and blocks the MC, which reduces the channel cross-section. A common way to measure the ion permselectivity of a channel is to measure its electric resistance. In a nonselective channel, the resistance is ohmic and constant for all electric currents. In contrast, in an ion-permselective channel, the resistance is constant only up to a threshold current, termed the limiting current (the terms underlimiting and overlimiting refer to currents below and above the limiting current, respectively). Above the limiting current, the electric resistance of the channel increases due to low ion concentration within the depletion layer. Thus, the deviation from constant electric resistance and the appearance of a limiting current are indications of channel ion permselectivity.[27,30,41,42]

Measurement of the current−voltage (I−V) through the channel as a function of the control channel pressures showed an I−V relation changing from a linear ohmic-like to a nonlinear behavior for control channel pressures of $P \leq 24$ psi

https://dx.doi.org/10.1021/acs.nanolett.0c02973
Nano Lett. 2020, 20, 8524−8533

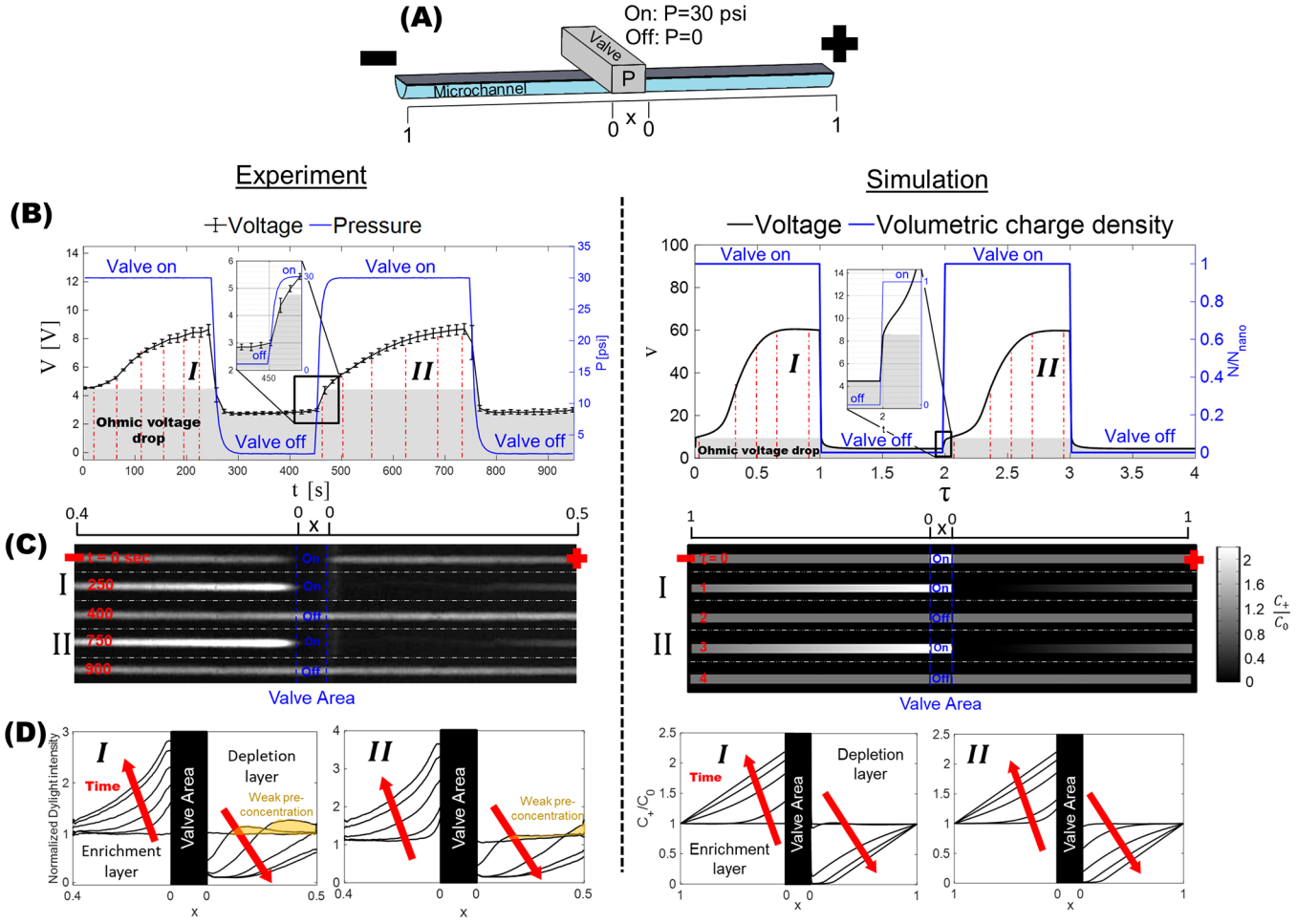

Figure 3. Dynamic response of a single tunable NC. The left column presents experimental results, while the right column presents the numerical simulation results. (A) Schematic description of the microfluidic channel with a single microvalve at its center. The valve was actuated and deactivated by changing the control channel pressure to P = 30 psi and P = 0 psi, respectively. (B) Experimental and numerical chronopotentiometric responses (i.e., voltage response for a constant applied current of $\sim 1.2 I_{lim}$) to a periodic pressure actuation of the microvalve (valve actuation at I, $0 < t < 250$ s; II, $450 < t < 750$ s). In the numerical simulation, the control channel pressure actuation was substituted by a stepwise application of the volumetric fixed charge (N), corresponding to the surface charge of the deformed valve. The gray region, in both experimental and numerical results, represents the ohmic resistance of the system in its deformed (actuated valve) and nondeformed (deactivated) microvalve state. (C) Experimental visualization of the fluorescence intensity along the MC as captured at t = 0, 250, 400, 750, and 900 s after applying the voltage (left column). The normalized cation concentration along the MC at τ = 0, 1, 2, 3, and 4, where τ is the time normalized by $2^{*}L^{2}_{micro}/D$ as calculated in the numerical simulation (right column). (D) The experimental normalized intensity profile of the fluorescence and the numerical normalized cation concentration, both at times corresponding to the dashed red lines depicted in part B. The experimentally measured intensity was normalized by the t = 0 s intensity, while the numerical cation concentration was normalized by initial cation concentration ($C_{+} = C_0$).

and $P \geq 28$ psi, respectively. In other words, for a pressure above 28 psi, the space underneath the microvalve is sufficiently small ($<\lambda_D$ = 12 nm at 0.65 mM) for the EDLs to overlap (Figure 2A). Next, we evaluated the NC height as a function of the control pressure by lowering the permselectivity of the NC. The NC permselectivity is reduced by increasing the solution conductivity to 130 mM KCl, thus shortening the Debye length (λ_D < 1 nm) and preventing the EDL overlap.[43] The ohmic resistance ($R^{nonselective}_{total}$) of the 2D model system, neglecting access resistances, can be described as two MC (R_{micro}) and a single NC ($R^{nonselective}_{nano}$) resistances connected in series

$$R_{micro} = \rho \frac{2L_{micro} - L_{control}F_{deform}}{H_{micro}WF_{shape}};$$

$$R^{nonselective}_{nano} = \rho \frac{L_{control}F_{deform}}{H_{nano}WF_{shape}} \quad (1)$$

$$R^{nonselective}_{total} = R_{micro} + R^{nonselective}_{nano} \quad (2)$$

where the averaged NC height, H_{nano}, is estimated as

$$H_{nano} = \frac{L_{control}F_{deform}}{WF_{shape}} \times \left[\frac{R^{nonselective}_{total}}{\rho} - \frac{2L_{micro} - L_{control}F_{deform}}{H_{micro}WF_{shape}}\right]^{-1} \quad (3)$$

with MC length, height, and width equal to L_{micro} = 4000 ± 100 μm, H_{micro} = 8 ± 1 μm, W = 35 ± 2 μm, respectively, and control channel length equal to $L_{control}$ = 50 ± 2 μm (described in Figure 1B). The 3D confocal scan (Figure 1C) demonstrated that only part of the membrane surface under the control channel was deformed and can be defined by the deformation factor F_{deform} = 0.9 ± 0.1. F_{shape} = 0.8 ± 0.1 expresses the deviation from a rectangular MC cross-section

https://dx.doi.org/10.1021/acs.nanolett.0c02973
Nano Lett. 2020, 20, 8524−8533

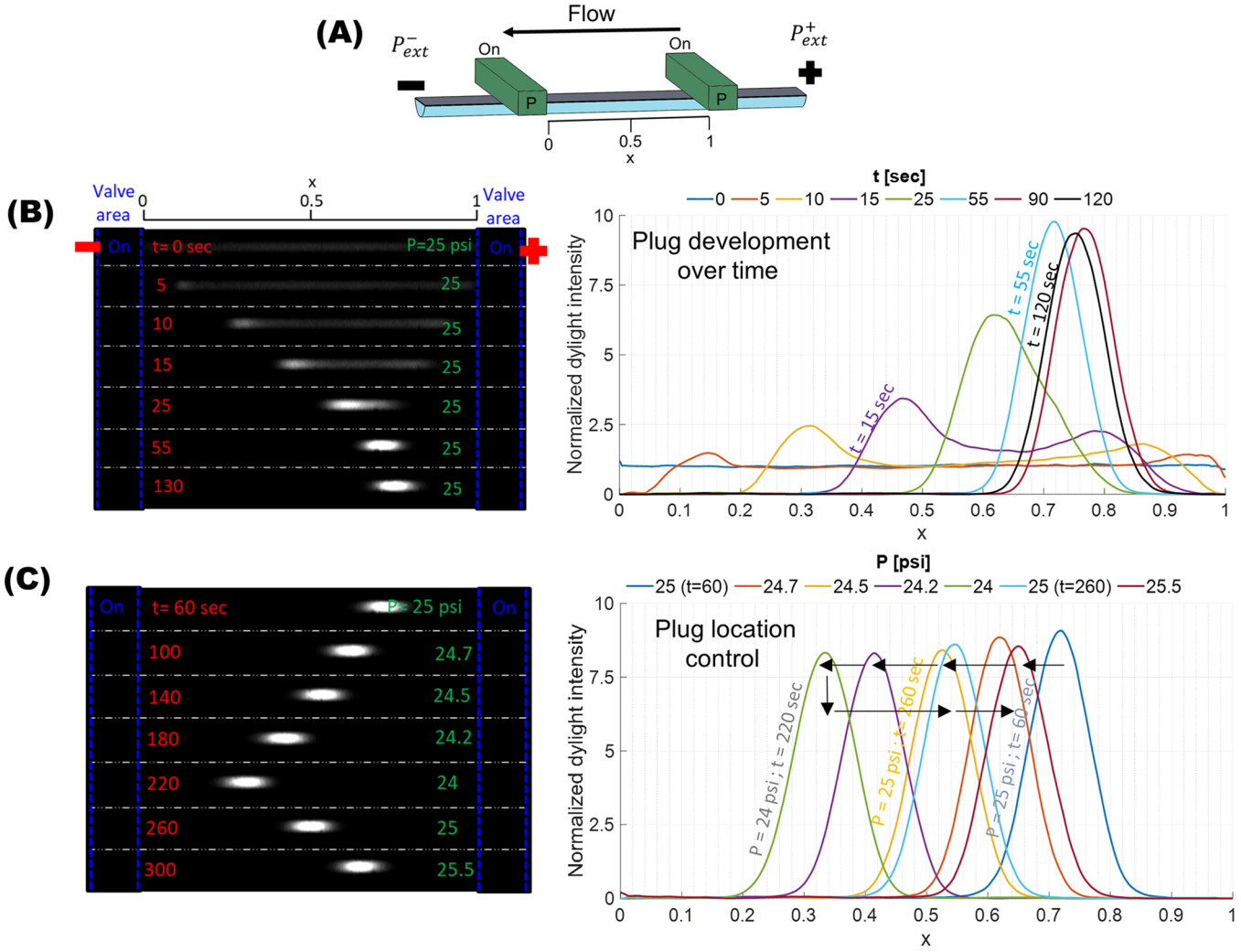

Figure 4. Experimental generation and manipulation of a preconcentration plug formed between two activated valves. (A) Schematic description of the experimental system, which contained two microvalves in series and flow from right to left, due to pressure difference ($P^+_{ext} > P^-_{ext}$). (B) Time-dependent fluorescence intensity profile under a constant valve pressure (P = 25 psi), external pressure drop ($P^+_{ext} > P^-_{ext}$) and electrical current ($I \approx 3I_{lim}$). The location and intensity of the formed plug changed over time. When the plug location stabilized (t > 55 s), its intensity was up to 10-fold higher than the initial intensity. The visualized oval-like shape of the preconcentration plug results from the semicircle cross sectional area of the main channel (for more information see Supplementary Figure S4). (C) Plug location, after stabilization, for different valve pressures (24 < P < 25.5 psi). Changing the valve pressure shifted the location of the plug (arrow) due to the change in the net flow through the MC (see Supplementary Video S4).

(evaluated based on the cross-section in Figure 1A) and $\rho = RT/(2DF^2C_0)$ is the electrical resistivity of the solution, where R = 8.314 J·mol/K and F = 96485 C/mol are the gas and Faraday constants, respectively, T is the temperature and C_0 is the bulk concentration.

This analysis demonstrates that the ohmic resistance of the system does not change for channel pressures up to P = 20 psi (Figure 2B, black line). At P = 25 psi, the resistance begins to increase, and the corresponding averaged NC height decreases (Figure 2B, red line), yet H_{nano} remains above 100 nm. With further increases in the control channel pressure, the average NC height decreases below 10 nm (Figure 2B), which verifies that the observed nonlinear behavior of the I−V relation is due to an EDL overlap ($H_{nano} < \lambda_D$ = 13 nm for $P \geq$ 28 psi at 0.65 mM) (Figure 2A). While this calculation assumes that the entire MC section underneath the membrane participates in the formation of the NC, in practice, some parts of it may be fully blocked, while others are higher than this average NC height.

The tunability of NC permselectivity was further characterized by performing a set of I−V measurements with varying concentration of ions and a constant control channel pressure of P = 30 psi (i.e., fixed NC height). The results showed increased ionic permselectivity with decreased solution conductivity and, accordingly, a shift from an ohmic-like to a nonlinear I−V response, as found in fixed-geometry NCs[27] (Supplementary Figure S2). In addition to verifying the CP phenomenon through the current response, the channel was visualized, using negatively charged fluorescent dye, during the I−V measurements. As expected, once the system reached its limiting current, the intensity near the anode side of the NC (depletion layer) significantly decreased, which indicates that the ion concentration decreased as well, while the intensity and the concentration at the cathode side increased (enrichment layer) (Supplementary Video S2).

These experimental observations were complemented by numerical simulations performed using a simplified 1D formulation (described in Supporting Information, numerical

https://dx.doi.org/10.1021/acs.nanolett.0c02973
Nano Lett. 2020, 20, 8524−8533

simulation section). As experimentally shown, reducing the channel's height resulted in an increase in the system's ohmic resistance. A further decrease in the channel height to a submicrometer size led to the appearance of ion permselectivity and a limiting current (Figure 2C).

To confirm the dependency of the system electrical response on the varying ionic permselectivity and electro-osmotic flow (EOF) with varying NC height,[44−45] a scaling relation of the normalized limiting current density that accounts for the presence of nonideal ionic permselectivity and effect of EOF advection on the CP was developed (see Supporting Information)[46,47]

$$i_{\mathrm{lim}} = i_{\mathrm{lim,ideal}}\left[\frac{\kappa+1}{\kappa-1}\right]\left[\frac{Pe}{e^{Pe}-1}\right] \quad (4)$$

where $Pe = -|\zeta\varepsilon_0\varepsilon_r\Delta V/(\mu D)|$ is EOF Péclet number (the minus sign is for the case of advection counteracting the diffusive propagation), ζ is the zeta potential, ε_0 and ε_r are the permittivity of vacuum and relative permittivity of water, respectively, ΔV is the voltage drop within the microchannel, μ is the water dynamic viscosity, D is the diffusion coefficient of the ionic species, κ is the ratio between the cation and anion fluxes within the NC, $(\kappa + 1)/(\kappa - 1)$ is a measure of the nonideal ionic permselectivity and approaches 1 for ideal selectivity, and $(Pe/(e^{Pe} - 1))$ stands for the deviation of the limiting current with EOF advection relative to that without $(i_{\mathrm{lim,ideal}})$.

Using this scaling relation (eq 4), we observe in Figure 2D that both experimental and numerical values collapse onto a line confirming the importance of the effects both nonideal permselectivity and advection have on the limiting current.

Dynamic Response of a Single Tunable Nanochannel. Next, the dynamic electrical and corresponding CP responses of a single tunable NC were experimentally investigated (Figure 3, left column). The former was obtained by measuring the voltage time response for an applied stepwise constant electrical current (i.e., chronopotentiometric response) (Figure 3B), while the latter was obtained by measuring the intensity profile of the fluorescent dye, which approximates the concentration changes of the background ions (Figure 3C,D). In contrast to the background ions of the dissolved salt that control the resistivity of the solution, the relatively low concentration of the fluorescent molecules have a negligible effect on the resistivity. The fluorescent molecules merely respond to the resulting electrical fields and thereby are used as an indicator of the background ion concentration. However, when combined with a counteracting convective force, the fluorescent molecules may preconcentrate, hence presenting dynamics that diverges from the changes exhibited by the background electrolyte ions, that is, exhibiting a third species behavior.[32]

The results clearly showed that upon application of the control channel pressure (P), the system's overall resistance increased from its open channel ohmic value, both due to the almost immediate decrease in the channel cross-section area under the deformed membrane and due to the time-dependent development of the ionic depletion layer, which adds to the electric resistance of the channel. The contribution of the ohmic resistance of the system includes the MC resistance when the valve is open ($250 < t < 450$ s, $t > 850$ s) and the formed NC, which is evaluated immediately after the membrane is deformed but before CP has developed (the gray area in Figure 3B). The maximum system resistance is obtained when the depletion layer is fully developed and the fluorescence intensity approaches zero, as expected when applying current higher than the limiting current ($I \approx 1.2I_{\mathrm{lim}}$, based on Figure 2A). Furthermore, visualization of the channel showed the development of the CP layer over time, with an increase in the fluorescence intensity near the cathode versus a decrease near the anode (Figure 3 C,D). Once the valve was released, the ion permselectivity vanished and the hydrodynamic resistance dropped, resulting in an increased solvent flow rate and rinsing of the channel with fresh solution. Therefore, the initial conditions can be recovered, as demonstrated in the second valve activation (II, $450 < t < 850$ s), which showed response similar to that of the first activation (I, $0 < t < 350$ s).

These observations were supported by the numerical simulation results (Figure 3, right column), where the control channel pressure changes translated to volumetric charge density changes (N), as described in the Supporting Information, numerical simulation section. However, the simulation omits the moderate intensity increase at the edge of the depletion layer, which is due to the formation of a preconcentration plug (represented by the yellow area in Figure 3D). Yet, since the net flow resulting from the EOF is not sufficient to rapidly accumulate many dye molecules and form a strong trap, the resulting intensity remains relatively low. This justifies neglecting convection in these numerical simulations, for simplification reasons.

Formation of an Array of Preconcentration Molecule Plugs. A preconcentrated plug of negatively (positively) charged analytes can be obtained at the edge of the depletion layer that is generated by a cation (anion) exchange medium as a result of counteracting convection and electro-migration forces. In the previous experiments (Figures 2 and 3), the EOF by itself was not sufficient to form a strong preconcentrated plug. Hence, the flow was increased (average velocity ~15 μm/s for deformed valve at $P = 26$ psi) by applying an external pressure drop ($P^{+}_{\mathrm{ext}} > P^{-}_{\mathrm{ext}}$) across the main MC inlets in the same direction as the induced EOF. For a single actuated valve, the preconcentrated plug location cannot be determined without an experimental precalibration process (see Supplementary Figure S3). However, for two activated microvalves in series (Figure 4A), following a transient stage of evolution of a stable preconcentrated plug between the two valves (Figure 4B), its location can be further tuned by changing the control channel pressure (Figure 4C). As clearly seen in Figure 4C, with decreasing system hydrodynamic resistance, due to decreased control channel pressure, the plug location is advected downstream and vice versa with increased pressure.

The applicability of the system to preconcentration of other bioparticles of varying size and electro-phoretic mobility, such as *E. coli*, avidin molecules, and biotin coated microparticles (0.8 μm), is seen in Supplementary Figure S5. The simultaneous preconcentration of avidin molecules and biotin coated microparticles and their spatial overlap, which resulted in an increased detection signal (Figure S5C,D) suggests the applicability of the device as a bead-based immunoassay where the locally tunable microchannel cross-section has a dual purpose, to control the ion permselectivity required for the formation of preconcentrated molecule plugs and to hydrodynamically trap the larger functionalized beads. Such dynamic control over the location of the preconcentrated plug is of marked importance for ensuring both the overlap between the

https://dx.doi.org/10.1021/acs.nanolett.0c02973
Nano Lett. 2020, 20, 8524−8533

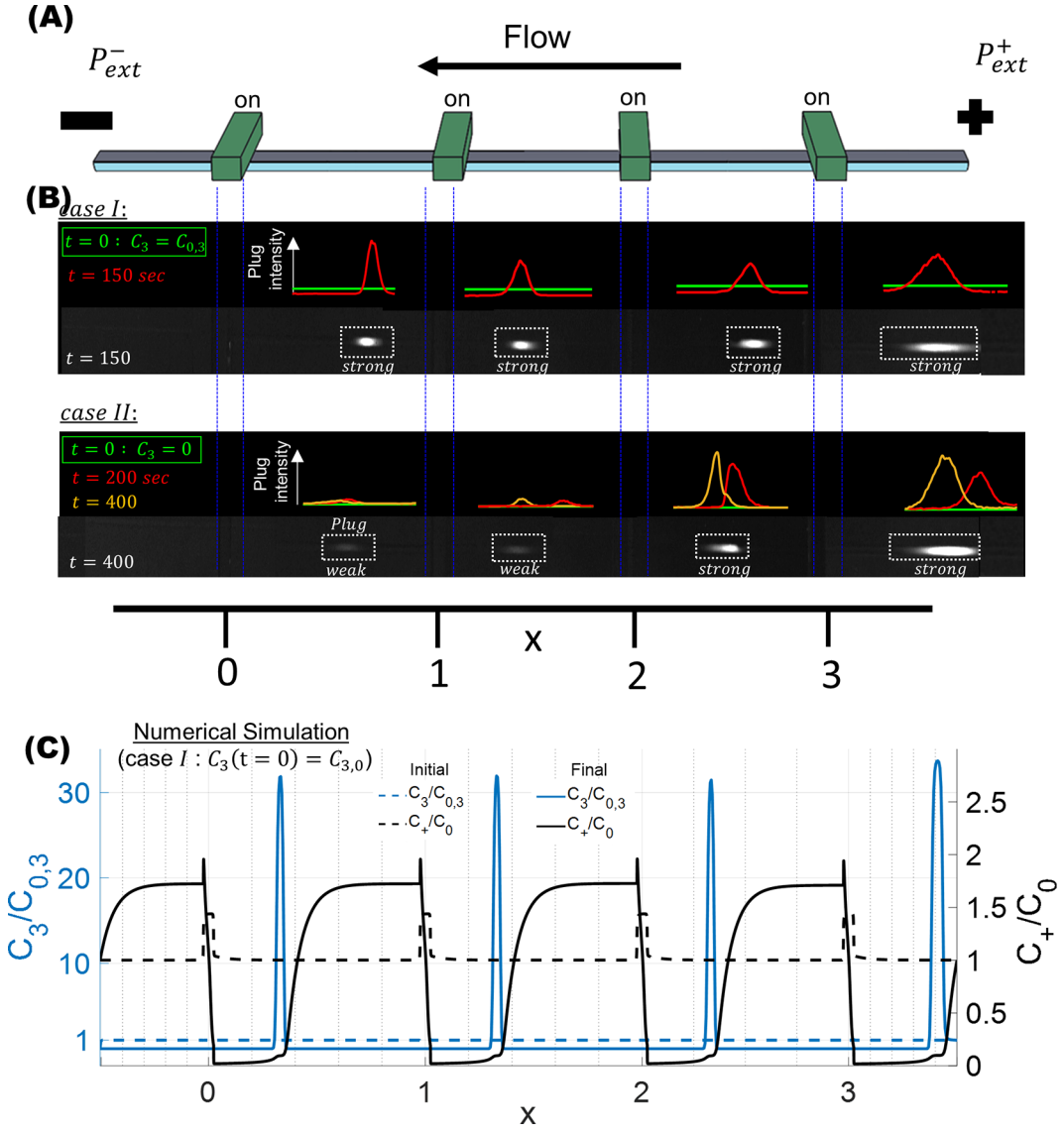

Figure 5. Multiple preconcentrated plugs that are simultaneously formed in series. (A) Schematic description of the experimental system, which contained four microvalves in series and flow from right to left, due to pressure difference ($P_{ext}^{+} > P_{ext}^{-}$). (B) Generation of four preconcentration plugs, for two different initial cases: a microchannel (MC) initially filled with fluorescent dye (case I, $C_3(t = 0) = C_{0,3}$) and a MC initially filled with deionized water (case II, $C_3(t = 0) = 0$). For both cases, fluorescent molecules were injected into the MC from the right inlet (for the dynamic response, see Supplementary Video S5). The channel visualization and the corresponding fluorescence intensity profiles near the plugs at different times are presented. (C) Simulation result of case I of four activated valves (valve location $x = 0, 1, 2, 3$), describing the normalized cation concentration (black line) and the normalized analyte concentration (C_3). The initial and final concentrations are represented by dashed and solid lines, respectively. The cation and analyte concentrations were normalized by the initial background concentration (C_0) and initial analyte concentration ($C_{0,3} = C_0/1000$), respectively.

preconcentrated plug of a target analyte and the sensing region (e.g., immobilized molecular probes on the surface or fixed beads, impedance/electrochemical sensor) and for multiplex sensing purposes.[48,49]

The ability to simultaneously form a series of preconcentrated plugs is of considerable importance for parallelization of biosensing. In addition, multiple traps connected in series provide for increased trapping efficiency of the target analyte that escaped the traps of the upstream formed preconcentrated plugs (Figure 5). As can be seen in Figure 5, preconcentrated plugs formed between each two valves and at the edge of the depletion layer (Figure 5C), with the analyte accumulation rate differing for each plug over time and with the number of plugs upstream and the initial analyte concentration. When the MC was completely filled with fluorescent dye from the very start (case I, $C_3(t = 0) = C_{0,3}$, similar to the above experiments), four almost identical plugs with high intensity developed simultaneously (Figure 5B). The number of plugs is hence controlled by the number of activated microvalves (see an example of deactivating one of the valves in Supplementary Figure S6 and Video S6). In contrast, when the channel was first filled with deionized water (DI) and the valves were fully deformed, the dye was injected into the right (anodic) inlet of the MC (case II, $C_3(t = 0) = 0$). Whereas the first upstream plug trapped most of the incoming analyte molecules, some managed to "escape" to the downstream plugs, which exhibited decreased fluorescence signals in accordance with their increased distance from the inlet. The formation of several

https://dx.doi.org/10.1021/acs.nanolett.0c02973
Nano Lett. 2020, 20, 8524−8533

preconcentration plugs in series for the initial conditions of uniform concentration of the analyte molecule is verified numerically (Figure 5C) and is in qualitative agreement with the experimental results.

CONCLUSIONS

This work demonstrated, for the first time, communication between two or more dynamically tunable NCs connected in series. The response of a single tunable NC to an applied electric current showed a strong dependency on the applied control channel pressure, with a shift from an ohmic to nonlinear electrical response (i.e., $I-V$), exhibiting a limiting current behavior. This resulted from the induced ionic permselectivity upon overlapping of Debye layers of the bottom and top microfluidic channel walls upon deformation of the membrane. The averaged NC height measured under ohmic conditions (i.e., when using a high concentration of salt) clearly showed the mechanical response of the microvalve and the formation of a nanoscale gap. Furthermore, the direct visualization of fluorescent molecules showed the development of the concentration-polarization phenomenon as a result of the ionic permselectivity. Periodic actuation of the microvalve further demonstrated the robustness and repeatability of NC tuning. Adding another tunable NC in series and applying a flow rate allowed for the simultaneous formation of multiple preconcentrated plugs. This dynamic tunability of the NCs adds important functionality to lab-on-a-chip devices, in particular, the ability to control the location of the preconcentrated plug. In addition, the ability to simultaneously form a series of preconcentrated plugs results in parallelization of the biosensing assay and increases the efficiency of target analyte trapping.

METHODS

Chip Fabrication. Polydimethylsiloxane (PDMS, SYLGARD 184, Dow Corning, USA) was cast on molding masters. The NCs were fabricated by bonding together three PDMS layers, the fluid channel, the membrane, and the control layer. The fluid channel master was made as previously described,[50] with some modification. In short, a 3 in. silicon wafer was baked at 120 °C for 15 min, followed by hexamethyldisilazane (HDMS) priming (1000 rpm, 45 s) to increase photoresist adhesion. Then, SPR 220 7.0 (Kayaku Advanced Materials, USA) was spun at 4000 rpm, 30 s. The wafers were then soft baked, at 105 °C for 7 min. The pattern was exposed via transparency photomask with 640 mJ/cm^2 of UV light (365 nm). The wafer was then left at room temperature for 2 h and then baked at 100 °C for 7 min. The wafer was then left at room temperature for 3 h to overnight and developed with a MICROPOSIT MF-CD-26 developer (Dow Chemical Company, USA) for 5 min. Next, the wafer was hard baked by gradually raising the hot plate temperature from 75 to 115 °C over 8 min. Finally, the wafer was heated to 150 °C for 5 min, followed by cooling on a 65 °C hot plate for 2 min. This reflowing process yielded semicircular ∼8 μm-high channels. The control channel master was made of a 3 in. silicon wafer, using standard photolithography, coated with a 300 μm layer of SU-8 photoresist (Microchem, USA).[51] The molding masters were designed using computer-aided design (CAD) software (AutoCad 2018, Autodesk, CA, USA). To prepare the membrane, a salinized silicon wafer was cleaned and activated with oxygen plasma and then vapor-salinized with trichloro(1*H*,1*H*,2*H*,2*H*-perfluorooctyl)silane (Sigma-Aldrich, USA) for 1 h. Next, the wafer was spin-coated with PDMS 20:1 (Base:Cross-linker) (1000 rpm, 60 s) and baked for 4 h on a 65 °C hot plate. This process yielded a membrane with a thickness of ∼100 μm.

Both the fluid and control master were cast with PDMS 10:1 and baked at 65 °C for more than 2 h. Once the PDMS cured, the molds were peeled off from the master and tubing and electrode holes were punched into the control slab only. The device was then bonded in two steps. First, the top side of the membrane was cleaned using a scotch tape and using oxygen plasma was bonded to the fluid slab and then baked in a 65 °C oven for >2 h. Second, the membrane and the fluid slab were carefully cut and peeled from the wafer. Third, the fluid-membrane and the control slabs were plasma-exposed, aligned, and bonded together. Finally, the device was baked in a 65 °C oven for >2 h to finalize the bonding between the layers (for schematic see Supplementary Figure S7).

Experimental Setup. To pressurize the control channel, the purified water (DI) pressure was controlled by a closed loop control system for each microvalve, using a syringe pump (KDS Legato 200 series, KD scientific), pressure sensor (Digi-Key, 480-3339-ND), and programmable controller (LabView 2018). Two Ag/AgCl electrodes (A-M system, 0.015 in. diameter) were inserted in each reservoir, connected to a power supply (Keithley 2636) to generate an electric field by applying a constant current and voltage, and the resulting voltage and current, respectively, were simultaneously monitored (for schematic, see Supplementary Figure S8). A KCl solution, of varied ionic concentrations, was used as the electrolyte. To measure the ohmic system response, a relatively high salt concentration (130 mM) was used, thereby preventing an EDL overlap. In contrast, for generation of CP, the ionic concentration was lowered significantly (0.65 mM). To stabilize the MC surface properties, the device was wetted the night before the experiment with DI water, along with 0.01% v/v nonionic surfactant (Tween 20, Sigma-Aldrich) to improve wetting capabilities. For the experiment, a pH-free fluorescent Dylight molecule (Dylight 488, Thermo Scientific) were used as an analyte for visualization of the CP layers mixed in the KCl electrolyte, along with 0.01% v/v nonionic surfactant, with the fluorescent molecule concentration being at least 2 orders of magnitude lower than the electrolyte concentration. The MCs were then washed under a constant voltage, via EOF, until the electrical current was stabilized. In addition, before each measurement, a current–voltage ($I-V$) linear sweep was performed to monitor for any ohmic resistance changes. For characterization of a single tunable NC (Figure 2), the $I-V$ curves were obtained from a linear sweep voltammetry, with a sweep rate of 10 mV/s, from 0 to 20 V. The chronopotentiometric responses were obtained by applying a constant overlimiting current (Figure 3). Microscopy was performed using a spinning disc confocal system (Yokogawa CSU-X1) connected to a camera (Andor iXon3), which allowed for capture of images on different focal planes (z).

ASSOCIATED CONTENT

Supporting Information

The Supporting Information is available free of charge at https://pubs.acs.org/doi/10.1021/acs.nanolett.0c02973.

https://dx.doi.org/10.1021/acs.nanolett.0c02973
Nano Lett. 2020, 20, 8524−8533

Description of the numerical simulations, scaling analysis of the limiting current details, and Figures S1−S10 (PDF)

3D-reconstructed deformed membrane for varying applied valve pressures (AVI)

Simultaneous visualization of the concentration-polarization phenomenon and $I-V$ measurement of a single tunable nanochannel under a constant control channel pressure (AVI)

Dynamic response of the concentration-polarization phenomenon within a single tunable nanochannel under varying control channel pressures (AVI)

Dynamic response of a preconcentrated plug of fluorescent dye molecules formed between two tunable nanochannels under varying control channel pressures (AVI)

Montage video of the dynamic response of preconcentrated plugs simultaneously formed within a system of four tunable nanochannels connected in series (AVI)

Scanning video the dynamic response of preconcentrated plugs simultaneously formed within a system of four and three tunable nanochannels connected in series (AVI)

AUTHOR INFORMATION

Corresponding Author

Gilad Yossifon − *Faculty of Mechanical Engineering, Micro- and Nanofluidics Laboratory, Technion−Israel Institute of Technology, Technion City 32000, Israel;* orcid.org/0000-0001-7999-2919; Email: yossifon@tx.technion.ac.il

Authors

Barak Sabbagh − *Faculty of Mechanical Engineering, Micro- and Nanofluidics Laboratory, Technion−Israel Institute of Technology, Technion City 32000, Israel*

Elad Stolovicki − *School of Engineering and Applied Sciences, Harvard University, Cambridge, Massachusetts 02138, United States*

Sinwook Park − *Faculty of Mechanical Engineering, Micro- and Nanofluidics Laboratory, Technion−Israel Institute of Technology, Technion City 32000, Israel*

David A. Weitz − *School of Engineering and Applied Sciences, Harvard University, Cambridge, Massachusetts 02138, United States;* orcid.org/0000-0001-6678-5208

Complete contact information is available at: https://pubs.acs.org/10.1021/acs.nanolett.0c02973

Author Contributions

G.Y., E.S. and B.S. conceived the idea of the study. B.S. performed the experiments, modeling, and numerics. E.S. and S.P. assisted in performing the experiments, data analysis, and chip fabrication. G.Y. supervised execution of experiments and data analysis. G.Y. and D.W. supervised planning of the study and the writing of the manuscript. All authors contributed to preparation of the manuscript.

Notes

The authors declare no competing financial interest.

ACKNOWLEDGMENTS

We acknowledge the support of the Israel Science Foundation (ISF 1938/16). We are grateful for the support of the National Science Foundation (DMR-1708729) and the National Science Foundation through the Harvard University MRSEC (DMR-1420570). This work was performed in part at the Center for Nanoscale Systems (CNS), a member of the National Nanotechnology Coordinated Infrastructure Network (NNCI), which is supported by the National Science Foundation under NSF award no. 1541959. CNS is part of Harvard University. We thank Sandra Nakasone, Guixiong Zhong, Jiangdong Deng, and all the other staff members at CNS for their useful advice and help in the device fabrication.

REFERENCES

(1) Kim, S. J.; Ko, S. H.; Kang, K. H.; Han, J. Direct seawater desalination by ion concentration polarization. *Nat. Nanotechnol.* **2010**, *5*, 297.

(2) Shannon, M. A.; et al. Science and technology for water purification in the coming decades. *Nature* **2008**, *452*, 301−310.

(3) Kwak, R.; Pham, V. S.; Kim, B.; Chen, L.; Han, J. Enhanced Salt Removal by Unipolar Ion Conduction in Ion Concentration Polarization Desalination. *Sci. Rep.* **2016**, *6*, 25349.

(4) Kim, B.; et al. Purification of High Salinity Brine by Multi-Stage Ion Concentration Polarization Desalination. *Sci. Rep.* **2016**, *6*, 31850.

(5) Guo, W.; et al. Energy harvesting with single-ion-selective nanopores: A concentration-gradient-driven nanofluidic power source. *Adv. Funct. Mater.* **2010**, *20*, 1339−1344.

(6) van der Heyden, F. H. J.; Bonthuis, D. J.; Stein, D.; Meyer, C.; Dekker, C. Electrokinetic Energy Conversion Efficiency in Nanofluidic Channels. *Nano Lett.* **2006**, *6*, 2232−2237.

(7) Li, R.; Fan, X.; Liu, Z.; Zhai, J. Smart Bioinspired Nanochannels and their Applications in Energy-Conversion Systems. *Adv. Mater.* **2017**, *29*, 1702983.

(8) Van Der Heyden, F. H. J.; Stein, D.; Dekker, C. Streaming Currents in a Single Nanofluidic Channel. *Phys. Rev. Lett.* **2005**, *95*, 116104.

(9) Kim, D.-K.; Duan, C.; Chen, Y.-F.; Majumdar, A. Power generation from concentration gradient by reverse electrodialysis in ion-selective nanochannels. *Microfluid. Nanofluid.* **2010**, *9*, 1215−1224.

(10) Jung, J. Y.; Joshi, P.; Petrossian, L.; Thornton, T. J.; Posner, J. D. Electromigration Current Rectification in a Cylindrical Nanopore Due to Asymmetric Concentration Polarization. *Anal. Chem.* **2009**, *81*, 3128−3133.

(11) Cheng, L.-J.; Guo, L. J. Nanofluidic diodes. *Chem. Soc. Rev.* **2010**, *39*, 923.

(12) Lee, H.; et al. A concentration-independent micro/nanofluidic active diode using an asymmetric ion concentration polarization layer. *Nanoscale* **2017**, *9*, 11871.

(13) Sun, G.; Senapati, S.; Chang, H.-C. High-flux ionic diodes, ionic transistors and ionic amplifiers based on external ion concentration polarization by an ion exchange membrane: a new scalable ionic circuit platform. *Lab Chip* **2016**, *16*, 1171.

(14) Song, H.; Wang, Y.; Garson, C.; Pant, K. Nafion-film-based micro-nanofluidic device for concurrent DNA preconcentration and separation in free solution. *Microfluid. Nanofluid.* **2014**, *17*, 693.

(15) Kim, M.; Jia, M.; Kim, T. Ion concentration polarization in a single and open microchannel induced by a surface-patterned perm-selective film. *Analyst* **2013**, *138*, 1370.

(16) Wang, Y.-C.; Stevens, A. L.; Han, J. Million-fold Preconcentration of Proteins and Peptides by Nanofluidic Filter. *Anal. Chem.* **2005**, *77*, 4293−4299.

(17) Han, S., II; et al. High-ionic-strength pre-concentration via ion concentration polarization for blood-based biofluids. *Sens. Actuators, B* **2018**, *268*, 485−493.

(18) Kwak, R.; Kim, S. J.; Han, J. Continuous-Flow Biomolecule and Cell Concentrator by Ion Concentration Polarization. *Anal. Chem.* **2011**, *83*, 7348−7355.

(19) Gong, M. M.; Nosrati, R.; San Gabriel, M. C.; Zini, A.; Sinton, D. Direct DNA Analysis with Paper-Based Ion Concentration Polarization. *J. Am. Chem. Soc.* **2015**, *137*, 13913.

(20) Fu, L. M.; Hou, H. H.; Chiu, P. H.; Yang, R. J. Sample preconcentration from dilute solutions on micro/nanofluidic platforms: A review. *Electrophoresis* **2018**, *39*, 289−310.
(21) Park, S.; Yossifon, G. Combining dielectrophoresis and concentration polarization-based preconcentration to enhance bead-based immunoassay sensitivity †. *Nanoscale* **2019**, *11*, 9436.
(22) Ko, S. H.; et al. Nanofluidic preconcentration device in a straight microchannel using ion concentration polarization. *Lab Chip* **2012**, *12*, 4472−4482.
(23) Lin, C.-C.; Hsu, J.-L.; Lee, G.-B. Sample preconcentration in microfluidic devices. *Microfluid. Nanofluid.* **2011**, *10*, 481.
(24) Fujikawa, T.; et al. Vibrations in Fluid−Structure Interaction Systems. *Flow-induced Vib.* **2014**, 359−401.
(25) McLaughlin, S. Electrostatic Potentials At Membrane-Solution Interfaces. *Curr. Top. Membr. Transp.* **1977**, *9*, 71−144.
(26) Manzanares, J. A.; Murphy, W. D.; Mafé, S.; Reiss, H. Numerical Simulation of the Nonequilibrium Diffuse Double Layer in Ion-Exchange Membranes. *J. Phys. Chem.* **1993**, *97*, 8524.
(27) Yossifon, G.; Mushenheim, P.; Chang, Y.-C.; Chang, H.-C. Nonlinear current-voltage characteristics of nanochannels. *Phys. Rev. E* **2009**, *79*, 046305.
(28) Mani, A.; Zangle, T. A.; Santiago, J. G. On the Propagation of Concentration Polarization from Microchannel-Nanochannel Interfaces Part I: Analytical Model and Characteristic Analysis. *Langmuir* **2009**, *25*, 3898.
(29) Schoch, R. B.; Han, J.; Renaud, P. Transport phenomena in nanofluidics. *Rev. Mod. Phys.* **2008**, *80*, 839.
(30) Rubinstein, I.; Shtilman, L. Voltage against Current Curves of Cation Exchange Membranes. *J. Chem. Soc., Faraday Trans. 2* **1979**, *75*, 231−246.
(31) Park, S.; Yossifon, G. Induced-charge electrokinetics, bipolar current, and concentration polarization in a microchannel-Nafion-membrane system. *Phys. Rev. E: Stat. Phys., Plasmas, Fluids, Relat. Interdiscip. Top.* **2016**, *93*, 062614.
(32) Park, S.; Yossifon, G. Electrothermal active control of preconcentrated biomolecule plugs. *Anal. Chem.* **2020**, *92*, 2476.
(33) Park, S.; Yossifon, G. Electrothermal based active control of ion transport in a microfluidic device with an ion-permselective membrane. *Nanoscale* **2018**, *10*, 11633.
(34) Mao, P.; Han, J. Massively-parallel ultra-high-aspect-ratio nanochannels as mesoporous membranes. *Lab Chip* **2009**, *9*, 586.
(35) Mijatovic, D.; Eijkel, J. C. T.; Van Den Berg, A. Technologies for nanofluidic systems: top-down vs. bottom-up-a review. *Lab Chip* **2005**, *5*, 492.
(36) Mao, P.; Han, J. Fabrication and characterization of 20 nm planar nanofluidic channels by glass-glass and glass-silicon bonding. *Lab Chip* **2005**, *5*, 837.
(37) Quist, J.; Trietsch, S. J.; Vulto, P.; Hankemeier, T. Elastomeric microvalves as tunable nanochannels for concentration polarization. *Lab Chip* **2013**, *13*, 4810.
(38) Cong, Y.; et al. Electrokinetic sample preconcentration and hydrodynamic sample injection for microchip electrophoresis using a pneumatic microvalve. *Electrophoresis* **2016**, *37*, 455−462.
(39) Kwon, H. J.; Hong, S. K.; Lee, M.; Lim, G. An on-demand micro/nano-convertible channel using an elastomeric nanostructure for multi-purpose use. *Lab Chip* **2019**, *19*, 2958.
(40) Kim, B.; et al. Tunable ionic transport for a triangular nanochannel in a polymeric nanofluidic system. *ACS Nano* **2013**, *7*, 740−747.
(41) Spiegler, K. S. Polarization at ion exchange membrane-solution interfaces. *Desalination* **1971**, *9*, 367−385.
(42) Yaroshchuk, A.; Yaroshchuk, A. What makes a nano-channel? *Microfluid. Nanofluid.* **2012**, *12*, 615−624.
(43) Green, Y.; Eshel, R.; Park, S.; Yossifon, G. Interplay between Nanochannel and Microchannel Resistances. *Nano Lett.* **2016**, *16*, 2744−2748.
(44) Chang, H.-C.; Yossifon, G.; Demekhin, E. A. Nanoscale Electrokinetics and Microvortices: How Microhydrodynamics Affects Nanofluidic Ion Flux. *Annu. Rev. Fluid Mech.* **2012**, *44*, 401−427.
(45) Zaltzman, B.; Rubinstein, I. Electro-osmotic slip and electro-convective instability. *J. Fluid Mech.* **2007**, *579*, 173−226.
(46) Rosentsvit, L.; Park, S.; Yossifon, G. Effect of advection on transient ion concentration-polarization phenomenon. *Phys. Rev. E: Stat. Phys., Plasmas, Fluids, Relat. Interdiscip. Top.* **2017**, *96*, 023104.
(47) Khair, A. S. Concentration polarization and second-kind electrokinetic instability at an ion-selective surface admitting normal flow. *Phys. Fluids* **2011**, *23*, 072003.
(48) Wang, Y.-C.; Han, J. Pre-binding dynamic range and sensitivity enhancement for immuno-sensors using nanofluidic preconcentrator. *Lab Chip* **2008**, *8*, 392−394.
(49) Freire, S. L. S.; Wheeler, A. R. Proteome-on-a-chip: Mirage, or on the horizon? *Lab Chip* **2006**, *6*, 1415−1423.
(50) Bartlett, N. W.; Wood, R. J. Comparative analysis of fabrication methods for achieving rounded microchannels in PDMS. *J. Micromech. Microeng.* **2016**, *26*, 115013.
(51) Qin, D.; Xia, Y.; Whitesides, G. M. Rapid prototyping of complex structures with feature sizes larger than 20 um. *Adv. Mater.* **1996**, *8*, 917−919.

https://dx.doi.org/10.1021/acs.nanolett.0c02973
Nano Lett. 2020, 20, 8524−8533